PCCP

Modeling Henry's Law and Phase Separations of Water-NaCl-Organic Mixtures with Solvation and Ion-Pairing

SCHOLARONE™
Manuscripts

Modeling Henry's Law and Phase Separations of Water-NaCl-Organic Mixtures with Solvation and Ion-Pairing

Aaron D. Wilson[a,*], Zi Hao Foo[b], Ashini S Jayasinghe[c], Caleb Stetson[a], Hyeonseok Lee[a], Harry W. Rollins[a], Akshay Deshmukh[b], John H. Lienhard[b]

[a] *Chemical Separations Group, Idaho National Laboratory, Idaho Falls, ID 83415-2208, USA*

[b] *Department of Mechanical Engineering, Massachusetts Institute of Technology, Cambridge, MA 02139-4307, USA*

[c] *Analytical Chemistry Group, Idaho National Laboratory, Idaho Falls, ID 83415-2208, USA*

* Email: aaron.wilson@inl.gov (A.D. Wilson)

Abstract

Empirical measurements of solution vapor pressure of ternary acetonitrile (MeCN) H_2O-NaCl-MeCN mixtures were recorded, with NaCl concentrations ranging from zero to the saturation limit, and MeCN concentrations ranging from zero to an absolute mole fraction of 0.64. After accounting for speciation, the variability of the Henry's law coefficient at vapor-liquid equilibrium (VLE) of MeCN ternary mixtures decreased from 107% to 5.1%. Solute speciation was modeled using a mass action solution model that incorporates solute solvation and ion-pairing phenomena. Two empirically determined equilibrium constants corresponding to solute dissociation and ion pairing were utilized for each solute. When speciation effects were considered, the solid-liquid equilibrium of H_2O-NaCl-MeCN mixtures appear to be governed by a simple saturation equilibrium constant that is consistent with the binary H_2O-NaCl saturation coefficient. Further, our results indicate that the precipitation of NaCl in the MeCN ternary mixtures was not governed by changes in the dielectric constant. Our model indicates that the compositions of the salt-induced liquid-liquid equilibrium (LLE) boundary of the H_2O-NaCl-MeCN mixture correspond to the binary plateau activity of MeCN, a range of concentrations over which the activity remains largely invariant in the binary water-MeCN system. Broader comparisons with other ternary miscible organic solvent (MOS) mixtures suggest that salt-induced liquid-liquid equilibrium exists if: 1) the solution displays a positive deviation from the ideal limits governed by Raoult's law; and 2) the minimum of the mixing free energy profile for the binary water-MOS system is organic-rich. This work is one of the first applications of speciation-based solution models to a ternary system, and the first that includes an organic solute.

1. Introduction

Solvent-driven fractional crystallization (SDFC) enables the efficient isolation and recovery of high-value metals and critical materials from brines and wastes.[1–4] In SDFC, a partially miscible organic solvent (MOS) induces fractional crystallization of dissolved inorganic ions at solid-liquid equilibrium.[5] However, unravelling the driving mechanism of solute-induced separations, is particularly challenging given the divergence of solution theory for electrolyte and non-electrolyte species.[6–9]

Contemporary approaches to model the interactions between water, salt, and organics include: 1) semi-empirical models based on the McMillan-Mayer (e.g., NRTL[10], UNIQUAC[11–13]) and Lewis-Randall (e.g., Pitzer-Debye-Hückel[14–16]) theories; and 2) fully empirical/Edisonian models based on Setschenow constants[17] or the Hofmeister series.[18] These models are efficacious in regressing and interpolating empirical data; however, they do not establish an underlying mechanism in which the regressed parameters directly correspond to a phenomenon, thereby lacking a correlative relationship.[19] Molecular dynamics (MDs) is a powerful means to understand complex mixtures involving water, salt, and organics systems on the intermolecular scale.[20] However, MD is challenged when predicting phase boundaries due to the length and time scales available for simulations as well as the interplay between "a mixture of strong (e.g., ion–ion) and weak (e.g., van der Waals) interactions" in complex mixtures.[20]

To bridge existing knowledge gaps, Zivitsas [6,7,21,22], Heyrokska [23–27], Reynolds [8,28–30], Wexler [31–35] and Wilson [5,9,36,37] have recently explored mechanistic mass action models that incorporate solvation and ion-pairing phenomena. Each of these models is distinct, with some approaches

60   retaining electrostatic terms. The implementation of ion pairing can occur before, after, or

61   concurrently with hydration and may impact the hydration model (e.g., decline in solvation upon

62   ion-pair formation). Ion pairing can be modeled with 1) conventional equilibria such as second-

63   order equilibrium for 1-1 and 2-2 salt, 2) unusual implementations such as concentration-

64   independent first-order dissociation (i.e., equilibrium coefficient corresponds to van 't Hoff

65   indices) or 3) the use of Debye-Hückel terms in lieu of ion-pairing.

66   Hydration has been modeled with three distinct approaches. First, through the application of

67   a concentration-independent hydration parameter. These fixed hydration values allow various

68   experimental data to be modeled across large concentration ranges. However, the model tends

69   to yield non-physical results at very high concentrations. Second, via equivalent-energy stepwise

70   hydration models, each hydration step of the solute can be treated as equal-energy reactions (e.g.,

71   identical equilibrium constants for each hydration step). This approach is premised on the

72   Brunauer–Emmett–Teller (BET) theory of vapor interacting with surfaces. The resulting models

73   predict statistical distributions of different degrees of solute hydration with the populations

74   varying with concentration.[38–41] Third, hydration can be modeled through the application of

75   stepwise hydration in which the energy of hydration changes with each hydration step of the

76   solute. Effectively, each successive removal of a hydrating water molecule from a solute requires

77   more energy than the previous step, analogous to the removal of protons from a polyacid with

78   multiple pK_a equilibrium values.[24,42] Based on this approach, the apparent degree of hydration

79   declines with solute concentration, a result which is attributed to a combination of changes in the

80   solute coordination environment and the joint solvation of solutes.[9] The degree of ion pairing and

81   hydration can be derived based on the geometry (e.g., coordination sphere) or the energy of an

82   interaction with the individual solute coordination environment while maintaining an average

83   energy of interaction.

84   Together with an expanded experimental dataset, we employ a mass action speciation

85   framework that incorporates second-order ion pairing and variable-energy stepwise solute

86   hydration[9] to correlate the solid-liquid and vapor-liquid equilibrium compositions of H_2O-NaCl-

87   MOS ternary mixtures. The model parameters are based on chemical equilibria that correlate

88   directly with physical phenomena. When NaCl and MOS are modeled as hydrates, we observe a

89   constant speciated NaCl mole fraction at solid liquid equilibrium (SLE) for MOS ternary mixtures.

90   Furthermore, our experiments suggest that the degree of NaCl crystallization is not driven directly

91   by MOS specific properties, such as dielectric constant[3] or surface tension.[43] At vapor-liquid

92   equilibrium (VLE), we found that the variability of the Henry's law coefficient for MeCN ternary

93   mixtures fell from 107% to 5.1% for NaCl concentrations ranging from 0 to saturation once solute

94   speciation is considered. Lastly, we discuss speciation implications for the composition of salt-

95   induced liquid-liquid equilibrium (LLE) and for the Gibbs free energy of mixing in ternary organic-

96   salt-water mixtures.

97   **1.1. Experimental Materials and Chemicals**

98   Nuclear magnetic resonance (NMR) spectra were acquired on a Bruker Avance III 600 MHz

99   spectrometer with a magnetic field strength of 14.093 T, corresponding to operating frequencies

100   of 600.13 MHz (^{1}H). All NMR experiments (except dimethyl ether) were captured with a co-axial

101   insert containing D_2O (Cambridge Isotopes Laboratories). The T1 of each integrated shift was

102   verified as generally below 2 s, with no shifts above 4 s observed. Na concentrations were

103   measured with inductively coupled plasma-optical emission spectroscopy (ICP-OES) at a detection

104   limit of 0.011 µg/mL Ca.

105   ACS-grade NaCl, free of anticaking agent, was used after being maintained for at least 48

106   hours in a vacuum oven at 150 °C. Solvents were obtained as anhydrous when possible. The MOS

107   used in these studies were dimethyl ether (DME), acetonitrile (MeCN), and *1,4*-dioxane. From NMR

108   experiments, the H_2O to MOS mole ratio was less than 0.001 for all the MOS used in this study.

109   **1.2. Aqueous Phase Composition of Water-NaCl-MOS**

110   Stock solutions with known masses of NaCl and distilled H_2O were prepared. The MOS was

111   added to 1-3 g of a stock NaCl solution. When the solution became cloudy, additions were slowed

112   until a thin organic layer was clearly visible upon settling. After settling, 0.4 mL of the heavier

113   aqueous phase was transferred to an NMR tube fitted with a coaxial insert containing D_2O. T1

114   experiments were conducted to establish the relaxation time of water and the MOS. Quantitative

115   NMR was conducted on the sample using 90-degree pulses, with delays (30-60 s) at least five

116   times longer than the longest T1 and temperature regulated at 298 K throughout. The mole ratio

117   of H_2O to MOS was established with NMR, while the mole ratio of water to NaCl was calculated

118   through species conservation.

119   **1.3. Temperature Dependent Vapor Pressure Measurements**

120   Vapor pressures of H_2O-NaCl-MeCN mixtures were determined using a Grabner Instruments

121   MINIVAP VPXpert vapor pressure analyzer using a triple expansion method at set temperatures

122   of 20.0, 25.0, and 30.0 °C with a 180 s equilibration time.

123   **2. Theory**

124   **2.1. Modeling Solute Speciation**

125   A mass action-based model premised on solvation and ion pairing was employed to model

126   the VLE behavior of the ternary mixtures.[9,36] The proposed framework correlates chemical

127   equilibrium compositions to the degree of solvation and ion pairing for organic and inorganic

128   solutes. Using two thermodynamic parameters for each inorganic salt, namely the equilibrium

129   constants for solute hydration and ion dissociation, the speciation-based model was successful in

130   regressing the VLE composition for 24 common 1-1 and 2-2 salts, with concentrations ranging

131   from infinite dilution to saturation.[9]

132   As a consequence of solute solvation and ion pairing, the effective solute mole fractions

133   depart from their corresponding absolute/anhydrous mole fractions. In the speciation model, as

134   depicted in Figure 1, the solvent energetically partitions into two distinct phases; the solvent exists

135   1) as part of the bulk phase (x_{H2O}^{Bulk}) or 2) as solvating molecules that are a part of the speciated

136   solutes ($x_B^{Solv.}$). This approach is consistent with the spatial response of solvents even in the

137   presence of a small amount of charged solute.[44]

138
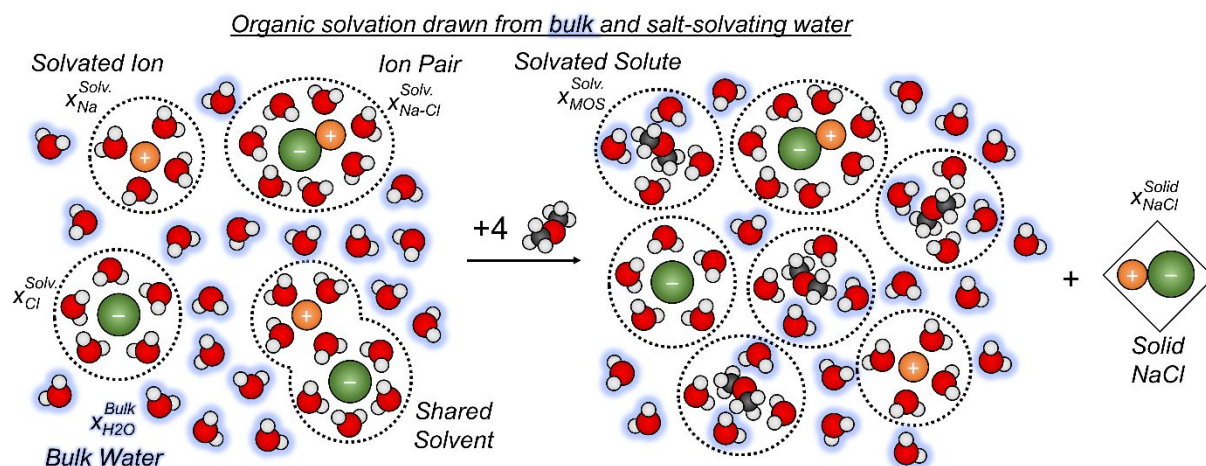
Figure 1: (Left) Saturated aqueous binary NaCl solution speciated based on $K_{NaCl}^{Hyd.}$ = 3.67 and $K_{NaCl}^{Dis.}$ = 0.033. (Right) The addition of a miscible organic solvent, namely DME in this illustration, ($K_{DME}^{Hyd.}$ = 3.55) results in precipitation of the NaCl. Here, the addition of DME induces a molar displacement of the solvated NaCl, precipitating it from the aqueous phase to maintain a constant speciated solute concentration at solid-liquid equilibrium. The solvation environment of DME is shaded in color to indicate the origins of its solvating water molecules relative to the saturated binary NaCl solution.

The absolute mole fraction of the inorganic ions was calculated with Equation 1, assuming full electrolyte dissociation of the salt.[9] By rearranging the equilibrium relationships, the solute's concentration-dependent degree of hydration can be calculated with Equation 2. Here, a hydration equilibrium constant ($K_B^{Hyd.}$) that is solute specific was employed.[9]

$$\left[x_B^{Abs.} \right] = \frac{\left[x_{B+}^{Abs.} \right] + \left[x_{B-}^{Abs.} \right]}{\left[x_{B+}^{Abs.} \right] + \left[x_{B-}^{Abs.} \right] + \left[x_{H2O}^{Abs.} \right] + \left[x_{MOS}^{Abs.} \right]} \tag{1}$$

$$n(H_2O)_B^{Hyd.} = K_B^{Hyd.} \left[x_{H2O}^{Abs.} \right]^m \tag{2}$$

For the H_2O-NaCl-MOS ternary mixtures investigated in this paper, the solvated mole fractions of NaCl ($\overline{x}_B^{Solv.}$) and the miscible organic solvent (MOS) ($\overline{x}_{MOS}^{Solv}$) were calculated with Equation 3. This formulation incorporates the solvating water molecules as part of the speciated solute mole fractions, by removing its contribution to the bulk solvent, as represented in the denominator of Equation 3:

$$\left[\overline{x}_B^{Solv.} \right] = \frac{\left[x_B^{Abs.} \right]}{\left[x_{H2O}^{Abs.} \right] + \left[x_{MOS}^{Abs.} \right] + \left[x_B^{Abs.} \right] - K_{MOS}^{Hyd.} \left[x_{H2O}^{Abs.} \right]^m \left[x_{MOS}^{Abs.} \right] - K_B^{Hyd.} \left[x_{H2O}^{Abs.} \right]^m \left[x_B^{Abs.} \right]} \tag{3}$$

For water molecules that are not involved in solvation, an equivalent expression was used to calculate the speciated bulk water mole fraction (x_{H2O}^{Bulk}), as shown in Equation 4:

$$\left[\overline{x}_{H2O}^{Bulk.} \right] = \frac{\left[x_{H2O}^{Abs.} \right] - K_{MOS}^{Hyd.} \left[x_{H2O}^{Abs.} \right]^m \left[x_{MOS}^{Abs.} \right] - K_B^{Hyd.} \left[x_{H2O}^{Abs.} \right]^m \left[x_B^{Abs.} \right]}{\left[x_{H2O}^{Abs.} \right] + \left[x_{MOS}^{Abs.} \right] + \left[x_B^{Abs.} \right] - K_{MOS}^{Hyd.} \left[x_{H2O}^{Abs.} \right]^m \left[x_{MOS}^{Abs.} \right] - K_B^{Hyd.} \left[x_{H2O}^{Abs.} \right]^m \left[x_B^{Abs.} \right]} \tag{4}$$

157

2.2. Incorporating Ion-Pairing Phenomena

159 The assumption of complete ionic dissociation is invoked by a majority of activity coefficient-

160 based models. Although these models successfully regress equilibrium data for inorganic

161 mixtures, poor model fidelity is often observed with mixtures of high ionic strength and valency,

162 or with mixed-solvent solutions.[45] In fact, Pitzer noted that the complete ion dissociation

163 conjecture was based on modeling convenience rather than on a mechanistic representation.[14]

164 Here, the ion-pairing phenomenon that dominates ion speciation was accounted for with the

165 appropriate equilibrium constants. For 1-1 electrolytes, which includes NaCl as used in this study,

166 the ionic equilibria between dissociated and associated ions can be represented by Equation 5,

167 where $K_B^{Dis.}$ denotes the ion dissociation equilibrium constant, and $\overline{x}_{B+}^{Solv.}$, $\overline{x}_{B-}^{Solv.}$ and $\overline{x}_{B\pm}^{Solv.}$ represent

168 the solvated mole fractions of Na$^+$ and Cl$^-$ ions, and Na-Cl ion pairs at equilibrium, respectively.

169 The effective mole fraction of the inorganic species $\left(\overline{x}_B^{Solv.}\right)$, which includes Na$^+$ and Cl$^-$ ions, and

170 Na-Cl ion pairs was computed with Equation 6.

$$K_B^{Dis.} = \frac{\left[\overline{x}_{B+}^{Solv.}\right]\left[\overline{x}_{B-}^{Solv.}\right]}{\left[\overline{x}_{B\pm}^{Solv.}\right]} \tag{5}$$

$$\left[\overline{x}_B^{Solv.}\right] = \left[\overline{x}_{B\pm}^{Solv.}\right] + \left[\overline{x}_{B+}^{Solv.}\right] + \left[\overline{x}_{B-}^{Solv.}\right] \tag{6}$$

171 Finally, the derived solvated mole fractions for H$_2$O, NaCl and MOS of the ternary mixtures

172 were renormalized to enable comparisons between the absolute and solvated mole fraction

173 frameworks, based on Equations 7 to 9.

$$\left[x_B^{Solv.}\right] = \frac{\left[\overline{x}_B^{Solv.}\right]}{\left[\overline{x}_B^{Solv.}\right] + \left[\overline{x}_{MOS}^{Solv.}\right] + \left[\overline{x}_{H2O}^{Bulk}\right]} \tag{7}$$

$$[x_{MOS}^{Solv.}] = \frac{[\bar{x}_{MOS}^{Solv.}]}{[\bar{x}_B^{Solv.}] + [\bar{x}_{MOS}^{Solv.}] + [\bar{x}_{H2O}^{Bulk}]} \tag{8}$$

$$[x_{H2O}^{Bulk}] = \frac{[\bar{x}_{H2O}^{Bulk}]}{[\bar{x}_B^{Solv.}] + [\bar{x}_{MOS}^{Solv.}] + [\bar{x}_{H2O}^{Bulk}]} \tag{9}$$

174

175 **2.3. Gibbs Free Energy Calculations**

176   Gibbs free energy calculation were based on Equation 10 with activities dependent on the

177 phase boundary domain, with a_n defined by Table 1.

$$g = x_x^{abs.} RT(a_n) \tag{10}$$

178   Over the SLE domain, the speciated concentrations were used to calculate the water and

179 electrolyte activity; the MOS activity was further modified with an average Henry's law coefficient.

180 Henry's law representatively connects infinite dilution activity with experimentally determined

181 saturation activity. Over the LLE domain, the activities of the MOS and electrolyte were estimated

182 with fixed saturation values; the water activity was the residual of MOS saturation and speciated

183 electrolyte fractions. The established MOS saturation activity is described in the Results and

184 Discussion section.

185 Table 1. Relationships used to calculate species activity, a_n.

Governing Relationship	Domain and Concentration Range
$a_{H2O} = x_{H2O}^{Solv.}$	SLE, $x_{MeCN} = 0 - 0.057$

$a_{NaCl} = x_{NaCl}^{Solv.}$	SLE, $x_{MeCN} = 0 - 0.057$
$a_{MOS} = x_{MeCN}^{Solv.} \times k_{MeCN}^{Solv.}$	SLE, $x_{MeCN} = 0 - 0.057$ $k_{MeCN}^{Solv.} = 6.4$
$a_{H2O} = 1 - x_{NaCl}^{Solv.} - x_{MeCN}^{Sat.}$	LLE, $x_{MeCN} = 0.057 - 0.800$ $x_{MeCN}^{Sat.} = 0.1$
$a_{NaCl} = a_{NaCl}^{Sat.} = 0.247$	LLE, $x_{MeCN} = 0.057 - 0.800$
$a_{MeCN} = a_{MeCN}^{Sat.} = 0.80$	LLE, $x_{MeCN} = 0.057 - 0.800$

186

3.   Results and Discussion

3.1. Implications on Solvent-induced Solid-Liquid Equilibria Boundary

189   The ion dissociation ($K_B^{Dis.}$) and hydration ($K_B^{Hyd.}$) equilibrium constants for NaCl were

190   regressed from the VLE data for binary H_2O-NaCl solutions, such that solvated mole fraction was

191   equal to the NaCl activity, as described in our prior work.[9] The corresponding ion dissociation and

192   hydration equilibrium constants for DME, MeCN, and dioxane were derived from the aqueous

193   phase composition of ternary H_2O-NaCl-MOS mixtures obtained in this and prior work. MeCN

194   and dioxane were selected because they represent fully miscible solvents with and without salt-

195   induced LLE with significant differences in dielectric constant and molecular mass. DME was

196   selected because it is a partially miscible solvent with a salt-induced LLE and is a strong candidate

197   for SDFC water treatment and mineral recovery applications.[1,2,5]
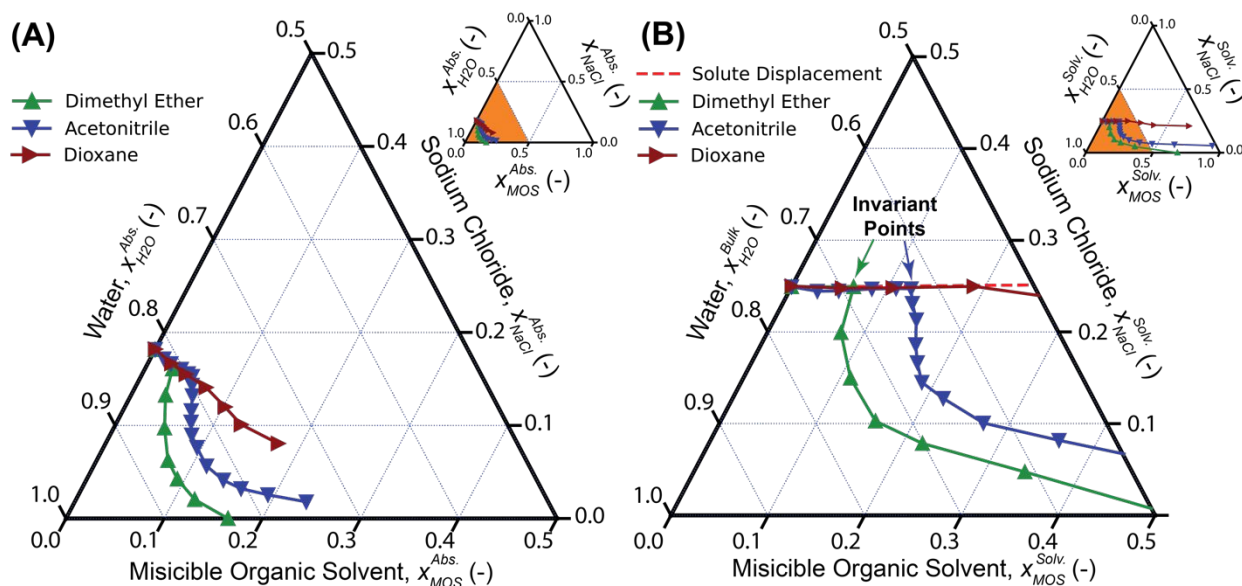
Figure 2: (A) Ternary phase diagram illustrating the aqueous-phase composition of the SLE boundary of H_2O-NaCl-MOS ternary mixtures for DME, MeCN, and 1,4-dioxane. The mole fractions correspond to the absolute scale, employing conventional full ion dissociation assumptions; **(B)** Ternary phase diagram illustrating the corresponding aqueous-phase composition of SLE boundaries of same H_2O-NaCl-MOS ternary mixtures, evaluated using the speciated mole fractions. The red line indicates the ideal molar displacement phenomenon observed with trace addition of MOS to a saturated binary NaCl solution. A constant speciated water mole fraction was observed with the addition of MOS, from the binary NaCl SLE to the respective invariant points. The model suggests that MOS addition draws solvating waters from the originally solvated NaCl ion pairs, causing solvent-induced SLE. The respective ion dissociation and hydration equilibrium constants used are: $K_{NaCl}^{Hyd.}$= 3.67, $K_{NaCl}^{Dis.}$ = 0.033, $K_{DME}^{Hyd.}$ = 3.55, $K_{MeCN}^{Hyd.}$= 2.85, $K_{Dioxane}^{Hyd.}$= 3.00.

The SLE composition for H_2O-NaCl-DME, H_2O-NaCl-MeCN and H_2O-NaCl-Dioxane ternary mixtures under the absolute mole fraction framework is depicted in Figure 2A. Using the speciation-based model incorporating hydration of the organic solute, the corresponding solvated mole fractions for the same ternary mixtures are presented in Figure 2B.

This speciation-based solution model treats both MOS and NaCl solutes as solvated in water. The dissolved solutes may interact with water through coordinating (e.g., hydrogen bonds) or non-coordinating mechanisms (i.e., when the water is not required to bond with the solute to solvate the solute, such as the formation of clathrate structures), or via a combination of processes.[36,37] In the speciated description of a saturated NaCl system (Figure 1 Left), roughly half

218   the water molecules exist as in the bulk (~55%) while the other half (~45%) are involved in NaCl

219   solvation. In the same solution environment ion pairing between Na-Cl dominates, with over 66%

220   of the Na^+ and Cl^- ions existing as ion pairs. At the molecular scale, when an MOS is added to a

221   saturated aqueous NaCl solution, the MOS is solvated by drawing water from the NaCl's solvation

222   environment.

223   In Figure 2B, once solute speciation has been incorporated, we observed an ideal molar

224   displacement relationship that is largely parallel to a solvated NaCl mole fraction of approximately

225   0.25, remaining constant between the saturated binary NaCl SLE and the respective MOS invariant

226   points. The degree of organic solute hydration was adjusted to match the idealized displacement

227   relationship between MOS and NaCl, as represented by the linear relationship (red line). This

228   suggests that once the solutes are fully speciated, the concentration of NaCl is constant in the

229   presence of varying organic solute concentrations. Therefore, it appears that when the MOS is

230   added to the saturated NaCl solution, the MOS draws water from the speciated NaCl ion pairs

231   and bulk water, increasing the speciated concentration of NaCl. According to the model, NaCl

232   precipitates upon MOS addition to maintain a constant speciated NaCl concentration (i.e.,

233   speciated solubility constant, K_{sp}, is independent of MOS concentration).

234   The displacement of NaCl by MOS was observed for all three ternary mixtures.[5] A K_{sp}

235   defining the SLE boundary and the implication of ideal molar behavior is surprising, given that

236   concentrated salts and dilute MOS solutions are generally known to be thermodynamically non-

237   ideal. In this case, NaCl deviates modestly with rational activity coefficients of 1.25[49,50] while MeCN

238   is far from ideal with a rational activity coefficient of 13.5.[51]

239   For the ternary mixtures containing MeCN or DME, we observed an invariant point in their

240   liquid phase boundary at the transition between SLE and LLE. The invariant point is the physical

241   condition where the further addition of MOS does not result in a decline of NaCl concentration

242   via solvent-induced crystallization of salt (SLE).[52,53] Likewise, further addition of NaCl does not

243   result in MOS concentration decline via salt-induced displacement of MOS (LLE).[52,53] In contrast,

244   the dioxane mixtures do not display a salt-induced LLE despite having a lower dielectric constant

245   than MeCN (i.e., ε of 2.1 vs. 36.6).[54] Further, dioxanes can fractionally crystallize ammonium sulfate

246   whereas nine out of thirteen polar solvents with a higher dielectric constant are incapable of

247   crystallizing ammonium sulfate under the same conditions.[55] Based on these observations, and

248   in contrast with common rationalizations in the literature,[56–58] the NaCl precipitation in these

249   ternary mixtures appears to not be driven by solvent polarity as conceived by a primitive non-

250   explicit model of a solution. To better understand these systems an in-depth study of the H_2O-

251   NaCl-MeCN ternary mixture has been conducted. The MeCN system was selected for these studies

252   in part as a proxy for DME (which has potential in SDFC applications[1,2,5]) because MeCN displays

253   a salt-induced LLE, like DME, but MeCN is a liquid at ambient conditions, in contrast to DME being

254   a gas. The concentrations and property measurements of H_2O-NaCl-MeCN systems can be more

255   accurately measured and controlled than H_2O-NaCl-DME systems because MeCN is a liquid.

256   **3.2. Invariability of Henry's Law Coefficients at Vapor-Liquid Equilibrium**

257   Figure 3A depicts the empirical vapor pressure of H_2O-NaCl-MeCN ternary mixtures, plotted

258   based on an absolute mole fraction basis. In the figure, MeCN was added to a binary H_2O-NaCl

259   mixture, for NaCl concentrations ranging from 0 (pure water) to its binary saturation value. At a

260   solution temperature of 298 K, the vapor pressure of pure MeCN is 12.2 kPa, as compared to the

261   vapor pressure of H_2O at 3.17 kPa. As expected from Henry's law, the addition of MOS induces a

262   linear increment in the solution vapor pressure. The gradient of the linear relationship between

263   the vapor pressure and the MeCN concentration (here evaluated on the absolute scale) is used to

264   calculate the Henry's law coefficient for the H_2O-NaCl-MeCN ternary mixture.

265   The apparent Henry's law coefficient is plotted against the initial NaCl concentrations in

266   Figure 3B, for NaCl concentrations ranging from zero to the binary saturation value. The derived

267   Henry's law coefficient appears to increase with NaCl concentrations, increasing from 816.0 kPa

268   with pure H_2O to 1,689 kPa with saturated NaCl solutions when visualized in absolute mole

269   fractions. A strong linear relationship between the Henry's law coefficient and the initial absolute

270   NaCl mole fraction is evident.

271   Based on classical solution thermodynamics at VLE, the fugacity of H_2O and MeCN are equal

272   between the vapor and the liquid phases.[51] When a small amount of MeCN is added to a NaCl

273   solution, the change in the liquid-phase fugacity of H_2O and MeCN results in a corresponding

274   change to the vapor-phase fugacity. The observed difference in the fugacity shift with varying

275   NaCl concentrations is conventionally rationalized with concentration-dependent fugacity

276   coefficients, which are dimensionless parameters describing the deviations of the vapor pressure

277   from the expected values of an ideal mixture.

278   The vapor pressure of the ternary mixture can be reevaluated against the speciated MeCN

279   mole fractions, as depicted in Figure 3C. The vertical intercepts in the figure correspond to the

280   vapor pressure of the respective binary NaCl solutions. Once speciation effects are incorporated,

281   we observed that the apparent Henry's law coefficients become largely consistent and invariant

282   to the initial NaCl concentrations, averaging 766.5 ± 38.9 kPa, as evident by the parallel linear

283   relationships. This observation is in agreement with recent reports demonstrating alignment with

284   ideal mixing laws even at high solute concentrations, after incorporating speciation effects.[31,32]

285   The concentration-dependent vapor pressures of H_2O–NaCl and H_2O–NaCl–MeCN are

286   plotted in Figure 3D. Between the two mixtures under the absolute scale, we observed a rise in

287   the apparent vapor pressure for a given MeCN mole fraction, as indicated by the first (H_2O-MeCN

288   Speciated) and third (H_2O-MeCN-NaCl Absolute) series plotted in the figure panel. Of note, when

289   the vapor pressures are reassessed with the speciated mole fractions, the apparent vapor pressure

290   of the ternary mixtures deviates less than 4% from the binary values. In sum, the result suggests

291   that a speciation-based solution theory successfully predicts the vapor pressure of

292   thermodynamically non-ideal mixtures and can potentially be applied to model VLE without

293   fugacity coefficients.
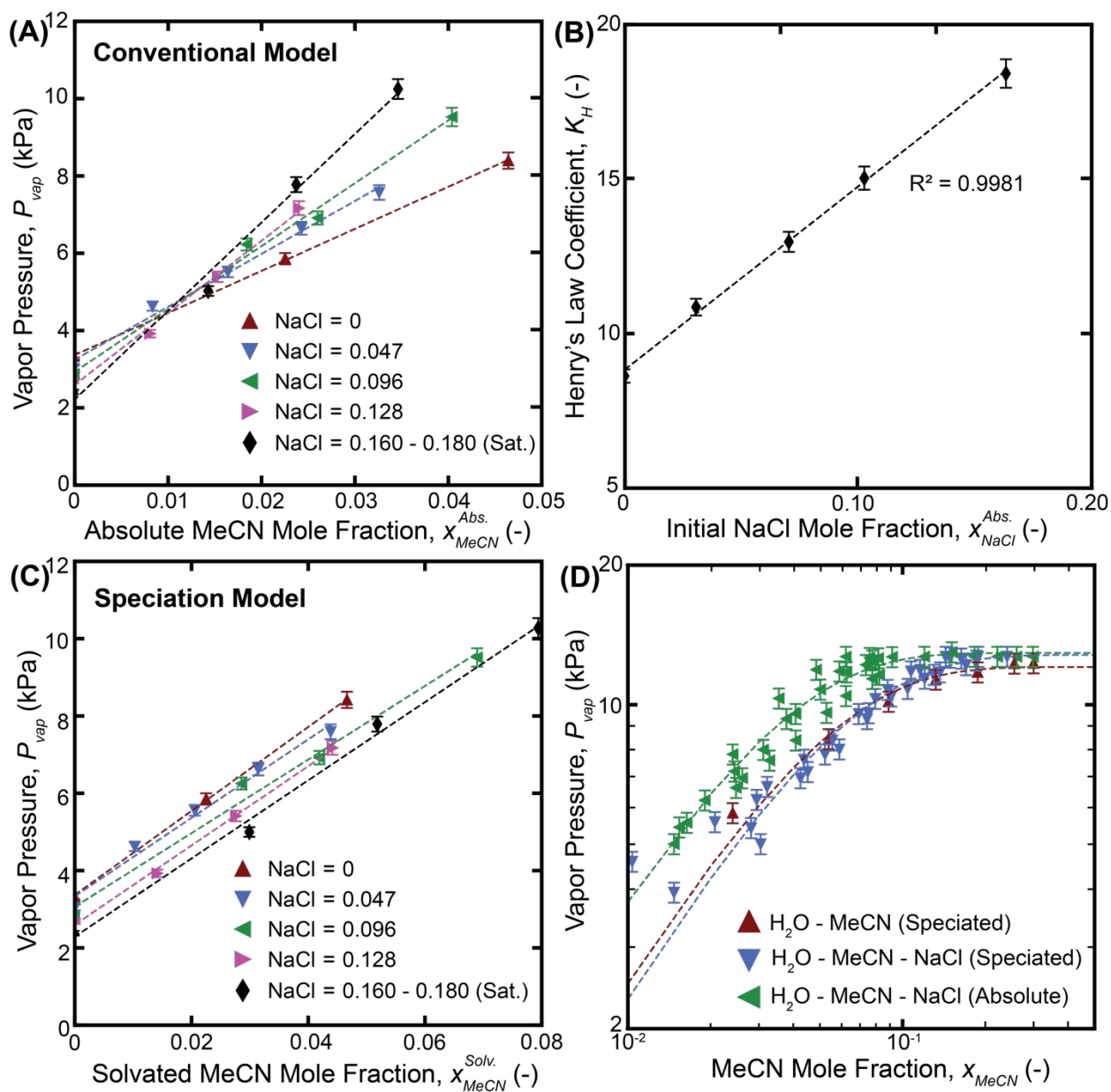
Figure 3 (A) Measured vapor pressures for ternary compositions of H_2O-NaCl-MeCN mixtures plotted against the absolute mole fraction concentration of MeCN for a series of initial NaCl to H_2O ratios. The slope is the Henry's Law volatility constant, K_H; **(B)** K_H plotted against the residual of the initial water activity of the binary water-NaCl fraction; **(C)** Measured vapor pressures for ternary H_2O-NaCl-MeCN mixtures plotted against the speciated concentration mole fraction concentration of MeCN. The derived Henry's law coefficient appears to be invariant with initial NaCl concentration and is consistent across a concentration range from pure water to binary saturation; **(D)** Plot of the measured vapor pressure versus the mole fraction of binary H_2O-MeCN and ternary H_2O-NaCl-MeCN mixtures. Once speciation effects are incorporated, the apparent vapor pressure of the binary and ternary mixtures deviate less than 4% from the speciated mole fraction of MeCN.

305   Given the proposed interaction mechanism of the speciation-based solution theory the effect

306   of NaCl on the Henry's law constant of MeCN is suspected to affect 1,4-dioxane, DME, and other

307   organic solvents in similar manner. The Henry's law constant of an organic solute expresses the

308   relationship between concentration and activity which directly relates to partial liquid-liquid

309   miscibility and salt-induced LLE. Salt-induced LLE appears to prevent DME from crystallizing salts

310   out of solutions containing a threshold concentration of high-activity salt (salts that reduce the

311   activity of water below ~0.9). This threshold is defined by the influence of high-activity salts on

312   the activity/Henry's law constant of DME. Further studies are underway into the threshold for salt-

313   induced LLE in H_2O-salt-DME for various salts. The physical properties that make certain MOS

314   prone to NaCl-induced LLE and other salts are resistant to this LLE can be evaluated with

315   previously published data.

316   **3.3. Implications on Binary and Salt-induced Liquid-Liquid Equilibrium Composition**

317   In binary H_2O–MOS mixtures at liquid-liquid equilibrium (LLE), complementary saturated

318   compositions exist in both liquid phases, where chemical potentials of water and MOS are equal,

319   producing a condition of isoactivity. A binary mixture with an effective composition in between

320   the two saturation compositions at LLE will disproportionate into the two distinct liquid phases

321   because the intermediate concentration achieves a lower free energy of mixing than the resulting

322   two-phase system. Binary H_2O–MOS mixtures that form positive azeotropes are also likely to

323   exhibit salt-induced LLE in the presence of NaCl, including MOS like tetrahydrofuran,[59]

324   isopropanol,[60] and 2,2,2-triflouroethanol [61].

325   Positive azeotropes form due to positive deviations from an ideal linear Raoult's law behavior,

326   arising from hetero interactions (between H_2O and MOS) that are weaker than homo interactions

327   (between H_2O and H_2O, or MOS and MOS). This results in the activities of the components (a_{H2O}

328   and a_{MOS}) summing to a value greater than unity; any system in which the total activity is greater

329   than unity suggests the existence of two possible distinct phases on a supramolecular scale larger

330   than the solvation environment, even when the mixture appears to be fully miscible.[62] A growing

331   body of experimental evidence supports the existence of distinct supramolecular or micro-

332   heterogeneous solution states in conventional fully miscible solvent systems, such as the H_2O-

333   MeCN mixture.[62–64]

334   The transition from a partially to fully miscible binary mixture can be conceptualized as the

335   process of reducing the compositional difference between the minimum mixing energy states for

336   each of the two separate phases. However, a transition from a two-phase system to a fully mixed

337   single-phase solution requires a dramatic change on a molecular scale. It is likely that

338   supramolecular mixing with micro-heterogeneities would exist at an intermediate state between

339   a partially miscible and a fully mixed binary system. In the binary water-MeCN system, the

340   unambiguous aqueous phase is defined by a linear decline in the water activity at low MeCN

341   concentrations (1:1 correlation between activity and mole fraction based on Raoult's law).

342   Following this linear decline, the mixture enters a region in which the water and MeCN activities

343   plateau, with modest change in the activities with respect to the mole fractions, as depicted in

344   Figure 4A. Based on the conjecture of supramolecular phase segregation, there are likely two

345   micro-phases in this region, a water-rich and an organic-rich phase, which are distinct on length

346   scales of nanometers to micrometers. The changes in water and MeCN activity over the

347   supramolecular mixing region can be attributed to the changes in the relative ratio of the two

348   phases. This interpretation is also supported by a range of spectroscopic, diffraction,

349   computational, and theoretical evidence.[65]

350   In the binary H_2O-MeCN system, the MeCN concentration in the water-rich sub-micron phase

351   at LLE can be estimated from the inflection point of the H_2O activity, as denoted by the solid stars

352   in Figure 4A. For the aqueous-rich phase of the H_2O-MeCN system, this inflection point occurs for

353   water activities between 0.89 and 0.91, suggesting that the H_2O-rich phase is saturated with mole

354   fractions of MeCN ranging from 0.09 to 0.11. The derived molecular solubility values coincide with

355   predictions from Henry's law for MeCN with a solubility of 0.5 mol/(m^3·Pa), corresponding to a

356   0.099 mole fraction for MeCN 298 K, as denoted by the red marker at an activity of 1.0.[66] Similarly,

357   the MeCN molecular phase is saturated with a H_2O mole fraction between 0.17 and 0.19, aligning

358   with the projections from Henry's law for water, as depicted in Figure 4. The aqueous, organic,

359   and supramolecular transitions are also supported by Soft X-ray Absorption Spectroscopy.[67] These

360   micro-phase compositions also correlate to the MOS activity at the salt-induced LLE, which

361   corresponds to the pressure limit of the H_2O-NaCl-MeCN system in Figure 3D.

362
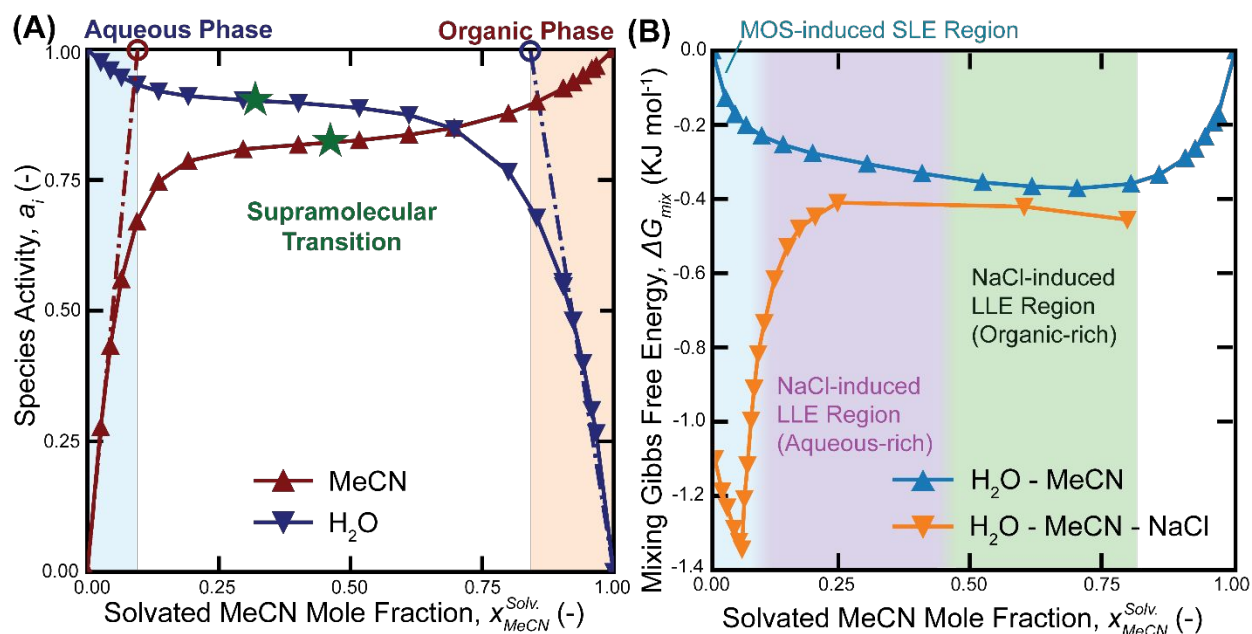
Figure 4 (A) Activity isotherm of binary H_2O-MeCN mixtures in VLE at 298.15 K.[68] The dashed traces relate to Henry's law and their pure component saturation points. Based on the division, the corresponding aqueous, organic, and supramolecular/microheterogeneity phases can be identified; **(B)** Plot of Gibbs free energy of mixing for binary H_2O-MeCN and ternary H_2O-MeCN-NaCl mixtures. The ternary data was calculated with Equation 10 and Table 1 with ternary data between 0.5 and 0.85 MeCN drawn from literature.[69] The free energy of mixing for the ternary mixtures displays a minimum around MeCN mole fractions of 0.05 and 0.7, corresponding to the NaCl- and MeCN-rich phases, respectively.

370

371   As illustrated in Figure 4B, the minimum mixing energy for binary H_2O-MeCN mixtures is

372   located at a MeCN mole fraction of 0.7. For ternary H_2O-NaCl-MOS mixtures, in general, the Gibbs

373   free energy of mixing profile can have two minimum points, one associated with a high NaCl mole

374   fraction and another associated with a high MOS mole fraction. For MeCN ternary mixtures, the

375   local minima are located at MeCN mole fractions of 0.05 and ~0.80, creating two distinct free

376   energy minima.

377   Water-MOS mixtures that exhibit positive azeotropic phenomena do not necessarily display a

378   salt-induced LLE in a ternary water-NaCl-MOS mixture. For instance, the water-dioxane mixture

379   displays a positive azeotrope but does not achieve the two minima, likely due to the position of

380   the binary free-energy minimum, which is reported at a dioxane mole fraction of ~0.5.[70,71] Shifting

381   the MOS's organic-water energy minimum from an organic mole fraction of 0.7 (MeCN-Water) to

382   0.5 (dioxanes-water) is towards the salt-defined energy minimum in the ternary mixture (H_2O-

383   NaCl-MOS). The two minima associated with binary mixtures of H_2O-NaCl and H_2O-MOS are likely

384   convoluted in the ternary system (H_2O-NaCl-dioxane). A salt-induced LLE is not observed in water-

385   dioxane mixtures even though dioxane is less polar than MeCN.

386   Acetone and water displays mixed phenomenon with MOS-induced SLE occurring

387   simultaneously with LLE.[5] Similar to the mixtures with dioxane, the binary water-acetone energy

388   of mixing minimum exists at MOS mole fraction of ~0.5.[72] This suggests that the binary water-

389   MOS energy of mixing minimum must be at a MOS mole fraction of ~0.5 or less to avoid a salt-

390   induced LLE, and that salt-induced LLE is not a result of a low MOS affinity for water. Thus, a binary

391   water-MOS system whose energy of mixing minimum is: 1) shallow (positive deviation from the

392   Raoult's law ideal with a plateau suggesting microstructuring) and; 2) majority organic (i.e. MOS

393   mole fraction greater than ~0.5) should be able to produce a salt induced LLE, as is the case with

394   tetrahydrofuran,[73] isopropanol,[72] and 2,2,2-triflouroethanol.[74]

395   Despite identifying a relationship for micro-phase saturation and interpreting a salt's influence

396   on the Henry's law constant for an MOS, it is unlikely that a speciation-based solution model

397   (based on chemical equilibria alone) can fully characterize salt-induced LLE in H_2O-NaCl-MeCN

398   mixtures, given the microstructural basis of LLE. The salt-induced LLE is quantitatively challenging

399   to model for the same reason it is difficult to model the transition from Henry's law behavior of

400   activity to non-Henry's law activity. The challenges arise because the activity is defined by

401   molecular environments while the supramolecular environments, which involve collections of

402   molecules to form a minimal structural unit, are defined by higher order equilibrium functions that

403   are not easily reduced to lower order equilibrium expressions. The potential of percolation[19,75–77]

404   or Windsor Type III[78] phase theories to bridge the existing gaps for the microstructured mixtures

405   should be evaluated in future work.

406   **4. Conclusions**

407   This paper is the first application of a speciation-based model to correlate the vapor-liquid

408   and solid-liquid equilibria of ternary mixtures containing organic solutes. The model utilizes two

409   equilibrium constants for each solute, accounting for ion pairing and solute solvation phenomena.

410   Using speciated mole fractions, our results indicate that the solid-liquid equilibrium boundaries

411   of ternary H_2O-NaCl-MeCN mixtures are governed by a simple saturation equilibrium condition

412   that is consistent with the respective saturation coefficients of the binary mixtures. Furthermore,

413   the degree of NaCl precipitation appears to be uncorrelated with changes in the solution dielectric

414   behavior. Original measurements for the vapor pressure of ternary H_2O-NaCl-MeCN mixtures

415   were recorded, for NaCl mole fractions ranging from zero to saturation and MeCN mole fractions

416   ranging from 0 to 0.64 on an absolute mole fraction scale. At vapor-liquid equilibrium, the

417   variability of the Henry's law coefficient fell from 107% to 5.1% once speciation effects were taken

418   into account by the proposed model. Deeper analysis suggests that salt-induced liquid-liquid

419   equilibrium occurs in ternary mixtures where the MOS phase exhibits stronger interactions with

420   the water solute than the corresponding interactions between the water phase and the MOS

421   solute. The proposed speciation framework can be leveraged as a basis for future work to model

422   liquid-phase microheterogeneities for the prediction of salt-induced SLE, organic-induced LLE,

423   and VLE of ternary systems.

424 **Nomenclature**

Symbol	Description
a_n	Species activities defined by domains (Table 1)
a_x	Activity of solute NaCl or MOS
$K_x^{Hyd.}$	Hydration equilibrium constant of NaCl or MOS
$K_x^{Dis.}$	Ion-pair dissociation equilibrium constant of NaCl
k_{MOS}^{sol}	Average speciated Henry's Law constant
B	Sum electrolyte; meaning varies with superscript
$B+$	Cation
$B-$	Anion
$B\pm$	Modeled ion pair
g	Gibbs free energy
$n(H_2O)_B^{Hyd.}$	Concentration-dependent hydration variable
m	Hydration exponent
MOS	Miscible organic solvent
$x_x^{Abs.}$	Absolute concentration of NaCl or MOS
x_{H20}^{Bulk}	H_2O not energetically involved in solvation of solute
$x_x^{Sat.}$	Saturated concentration
$\overline{x}_x^{Solv.}$	Unnormalized speciated concentration of NaCl or MOS
$x_x^{Solv.}$	Speciated concentration of NaCl or MOS

425

426 **Author Contributions**

427   **A.D. Wilson**: Conceptualization, Computation, Formal Analysis, Writing – Original Draft; **Z.H. Foo**:

428   Visualization, Computation, Formal Analysis, Writing – Original Sections; **A.S. Jayasinghe, C.**

429   **Stetson, H. Lee, H.W. Rollins**: Experiment, Writing – Review and Editing; **A. Deshmukh, J.H.**

430   **Lienhard**: Formal Analysis, Writing – Review and Editing

431   **Conflicts of Interest**

432   The authors declare no conflicts of interest that may have appeared to influence the content of

433   this paper.

434   **Acknowledgement**

438   **References**
439

440   1   C. Stetson, D. Prodius, H. Lee, C. Orme, B. White, H. Rollins, D. Ginosar, I. C. Nlebedim and A. D.
441   Wilson, Solvent-driven fractional crystallization for atom-efficient separation of metal salts from
442   permanent magnet leachates, *Nat. Commun.*, 2022, **13**, 3789.
443   2   Z. H. Foo, C. Stetson, E. Dach, A. Deshmukh, H. Lee, A. K. Menon, R. Prasher, N. Y. Yip, J. H. Lienhard
444   and A. D. Wilson, Solvent-driven aqueous separations for hypersaline brine concentration and
445   resource recovery, *Trends Chem.*, 2022, **4**, 1078–1093.
446   3   Y. Ma, M. Svärd, X. Xiao, J. M. Gardner, R. T. Olsson and K. Forsberg, Precipitation and Crystallization
447   Used in the Production of Metal Salts for Li-Ion Battery Materials: A Review, *Metals*, 2020, **10**, 1609.
448   4   C. Boo, H. Qi, I. H. Billinge, K. M. Shah, H. Fan and N. Y. Yip, Thermomorphic Hydrophilicity Base-
449   Induced Precipitation for Effective Descaling of Hypersaline Brines, *ACS EST Eng.*, 2021, **1**, 1351–1359.
450   5   J. S. McNally, Z. H. Foo, A. Deshmukh, C. J. Orme, J. H. Lienhard and A. D. Wilson, Solute displacement
451   in the aqueous phase of water-NaCl-organic ternary mixtures relevant to solvent-driven water
452   treatment, *RSC Adv.*, 2020, **10**, 29516–29527.
453   6   A. A. Zavitsas, Properties of water solutions of electrolytes and nonelectrolytes, *J. Phys. Chem. B*,
454   2001, **105**, 7805–7817.
455   7   A. A. Zavitsas, Properties of aqueous solutions. A treatise against osmotic and activity coefficients, *J.*
456   *Mol. Liq.*, 2022, **348**, 118410.

457   8   J. G. Reynolds, T. R. Graham and C. I. Pearce, Extending Zavitsas' hydration model to the
458   thermodynamics of solute mixtures in water, *J. Mol. Liq.*, , DOI:10.1016/j.molliq.2021.118309.
459   9   A. D. Wilson, H. Lee and C. Stetson, Mass action model of solution activity via speciation by solvation
460   and ion pairing equilibria, *Commun. Chem.*, 2021, **4**, 1–8.
461   10 G. M. Bollas, C. C. Chen and P. I. Barton, Refined electrolyte-NRTL model: Activity coefficient
462   expressions for application to multi-electrolyte systems, *AIChE J.*, 2008, **54**, 1608–1624.
463   11 M. C. Iliuta, K. Thomsen and P. Rasmussen, Extended UNIQUAC model for correlation and prediction
464   of vapour-liquid-solid equilibria in aqueous salt systems containing non-electrolytes. Part A.
465   methanol-water-salt systems, *Chem. Eng. Sci.*, 2000, **55**, 2673–2686.
466   12 A. Mohs and J. Gmehling, A revised LIQUAC and LIFAC model (LIQUAC*/LIFAC*) for the prediction of
467   properties of electrolyte containing solutions, *Fluid Phase Equilibria*, 2013, **337**, 311–322.
468   13 Z. H. Foo, D. Rehman, O. Z. Coombs, A. Deshmukh and J. H. Lienhard, Multicomponent Fickian
469   solution-diffusion model for osmotic transport through membranes, *J. Membr. Sci.*, 2021, **640**,
470   119819.
471   14 K. S. Pitzer, Thermodynamics of electrolytes. I. Theoretical basis and general equations, *J. Phys.*
472   *Chem.*, 1973, **77**, 268–277.
473   15 H. T. Kim and W. J. Frederick, Evaluation of Pitzer Ion Interaction Parameters of Aqueous Electrolytes
474   at 25°C. 1. Single Salt Parameters, *J. Chem. Eng. Data*, 1988, **33**, 177–184.
475   16 H. T. Kim and W. J. Frederick, Evaluation of pitzer ion interaction parameters of aqueous mixed
476   electrolyte solutions at 25 °C. 2. Ternary mixing parameters, *J. Chem. Eng. Data*, 1988, **33**, 278–283.
477   17 A. Burant, G. V. Lowry and A. K. Karamalidis, Measurement and Modeling of Setschenow Constants
478   for Selected Hydrophilic Compounds in NaCl and CaCl2 Simulated Carbon Storage Brines, *Acc. Chem.*
479   *Res.*, 2017, **50**, 1332–1341.
480   18 B. Kang, H. Tang, Z. Zhao and S. Song, Hofmeister Series: Insights of Ion Specificity from Amphiphilic
481   Assembly and Interface Property, *ACS Omega*, 2020, **5**, 6229–6239.
482   19 M. J. Servis, E. Martinez-Baez and A. E. Clark, Hierarchical phenomena in multicomponent liquids:
483   simulation methods, analysis, chemistry, *Phys. Chem. Chem. Phys.*, 2020, **22**, 9850–9874.
484   20 M. J. Servis, E. Martinez-Baez and A. E. Clark, Hierarchical phenomena in multicomponent liquids:
485   simulation methods, analysis, chemistry, *Phys. Chem. Chem. Phys.*, 2020, **22**, 9850–9874.
486   21 A. A. Zavitsas, Ideal behavior of water solutions of strong electrolytes and non-electrolytes at high
487   concentrations, *J. Solut. Chem.*, 2010, **39**, 301–317.
488   22 A. A. Zavitsas, The Nature of Aqueous Solutions: Insights into Multiple Facets of Chemistry and
489   Biochemistry from Freezing-Point Depressions, *Chem. – Eur. J.*, 2010, **16**, 5942–5960.
490   23 R. Heyrovska, Reappraisal of Arrhenius' theory of partial dissociation of electrolytes, *ACS Symp. Ser.*,
491   1989, 75–91.
492   24 R. Heyrovská, Degrees of Dissociation and Hydration Numbers of Alkali Halides in Aqueous Solutions
493   at 25 °C (Some up to Saturation), *Croat. Chem. Acta*, 1997, **70**, 39–54.
494   25 R. Heyrovská, Volumes of ions, ion pairs, and electrostriction of alkali halides in aqueous solutions at
495   25°C, *Mar. Chem.*, 2000, **70**, 49–59.
496   26 R. Heyrovská, Ionic Concentrations and Hydration Numbers of "Supporting Electrolytes",
497   *Electroanalysis*, 2006, **18**, 351–361.
498   27 R. Heyrovska, Partial Dissociation and Hydration Quantitatively Explain the Properties of Aqueous
499   Electrolyte Solutions and hence Empirical Activity Concepts are Unnecessary, *Nat. Preced. 2011*,
500   2011, 1–1.
501   28 J. G. Reynolds, A method to apply Zavitsas' aqueous electrolyte model to multicomponent solutions
502   and its equivalence to Zdanovskii's rule, *AIChE J.*, 2022, **68**, e17487.
503   29 J. G. Reynolds, Solubilities in aqueous nitrate solutions that appear to reverse the law of mass action,
504   *Phys. Chem. Chem. Phys.*, 2021, **23**, 21407–21418.

505   30 J. G. Reynolds and W. River, Correction: Solubilities in aqueous nitrate solutions that appear to
506   reverse the law of mass action, *Phys. Chem. Chem. Phys.*, 2021, **23**, 24061–24061.
507   31 A. S. Wexler, Raoult was right after all, *ACS Omega*, 2019, **4**, 12848–12852.
508   32 A. S. Wexler, Raoult was right after all: Statistical mechanics derivation and volumetric validation,
509   *Fluid Phase Equilibria*, 2021, **531**, 112899.
510   33 A. S. Wexler, A step-wise ion hydration model of aqueous electrolyte solution: The 1:1 punch, *Fluid*
511   *Phase Equilibria*, 2022, **559**, 113498.
512   34 A. S. Wexler, K. Patel, M. Gen and C. K. Chan, Reconciling Measurement and Prediction of Free and
513   Solvated Water in Solution, *ACS Omega*, 2020, **5**, 8754–8765.
514   35 R. A. Zaveri, R. C. Easter and A. S. Wexler, A new method for multicomponent activity coefficients of
515   electrolytes in aqueous atmospheric aerosols, *J. Geophys. Res. Atmospheres*, 2005, **110**, 1–23.
516   36 A. D. Wilson and C. Stetson, Modeling solution vapor equilibria with solvation and solute assembly, *J.*
517   *Mol. Liq.*, 2021, **336**, 116272.
518   37 A. D. Wilson, H. Lee and C. Stetson, Local stress within a granular molecular solvent matrix, a
519   mechanism for individual ion hydration, *J. Mol. Liq.*, 2022, 119544.
520   38 R. H. Stokes and R. A. Robinson, Ionic Hydration and Activity in Electrolyte Solutions, *J. Am. Chem.*
521   *Soc.*, 1948, **70**, 1870–1878.
522   39 R. H. Stokes and R. A. Robinson, Solvation equilibria in very concentrated electrolyte solutions, *J.*
523   *Solut. Chem.*, 1973, **2**, 173–191.
524   40 G. Scatchard, The Hydration of Sucrose in Water Solution as Calculated from Vapor-Pressure
525   Measurements., *J. Am. Chem. Soc.*, 1921, **43**, 2406–2418.
526   41 Y. Marcus, Concentration Dependence of Ionic Hydration Numbers, *J. Phys. Chem. B*, 2014, **118**,
527   10471–10476.
528   42 Y. Marcus, Concentration dependence of ionic hydration numbers, *J. Phys. Chem. B*, 2014, **118**,
529   10471–10476.
530   43 D. Chandler, Interfaces and the driving force of hydrophobic assembly, *Nature*, 2005, **437**, 640–647.
531   44 A. Montenegro, C. Dutta, M. Mammetkuliev, H. Shi, B. Hou, D. Bhattacharyya, B. Zhao, S. B. Cronin
532   and A. V. Benderskii, Asymmetric response of interfacial water to applied electric fields, *Nature*, 2021,
533   **594**, 62–65.
534   45 T. F. Anderson and J. M. Prausnitz, Application of the UNIQUAC Equation to Calculation of
535   Multicomponent Phase Equilibria. 1. Vapor-Liquid Equilibria, *Ind. Eng. Chem. Process Des. Dev.*, 1978,
536   **17**, 552–561.
537   46 C. Stetson, D. Prodius, H. Lee, C. Orme, B. White, H. Rollins, D. Ginosar, I. C. Nlebedim and A. D.
538   Wilson, Solvent-driven fractional crystallization for atom-efficient separation of metal salts from
539   permanent magnet leachates, *Nat. Commun.*, 2022, **13**, 3789.
540   47 Z. H. Foo, C. Stetson, E. Dach, A. Deshmukh, H. Lee, A. K. Menon, R. Prasher, N. Y. Yip, J. H. Lienhard
541   and A. D. Wilson, Solvent-driven aqueous separations for hypersaline brine concentration and
542   resource recovery, *Trends Chem.*, 2022, **4**, 1078–1093.
543   48 J. S. McNally, Z. H. Foo, A. Deshmukh, C. J. Orme, J. H. Lienhard and A. D. Wilson, Solute displacement
544   in the aqueous phase of water–NaCl–organic ternary mixtures relevant to solvent-driven water
545   treatment, *RSC Adv.*, 2020, **10**, 29516–29527.
546   49 B. P. Feeley, M. A. Overton, M. M. Galloway, T. J. Lecrivain and A. D. Wilson, Idaho Database of
547   Solution Thermodynamics, *J. Mol. Liq.*, 2021, 116574.
548   50 G. Scatchard, W. J. Hamer and S. E. Wood, Isotonic Solutions. I. The Chemical Potential of Water in
549   Aqueous Solutions of Sodium Chloride, Potassium Chloride, Sulfuric Acid, Sucrose, Urea and Glycerol
550   at 25°1, *J. Am. Chem. Soc.*, 1938, **60**, 3061–3070.

551 51 A. Deshmukh, Z. H. Foo, C. Stetson, H. Lee, C. J. Orme, A. D. Wilson and J. H. Lienhard,
552   Thermodynamics of solvent-driven water extraction from hypersaline brines using dimethyl ether,
553   *Chem. Eng. J.*, 2022, **434**, 134391.
554 52 F. Farelo, C. Fernandes and A. Avelino, Solubilities for six ternary systems: NaCl + NH4Cl + H 2O, KCl +
555   NH4Cl + H2O, NaCl + LiCl + H 2O, KCl + LiCl + H2O, NaCl + AlCl3 + H 2O, and KCl + AlCl3 + H2O at T =
556   (298 to 333) K, *J. Chem. Eng. Data*, 2005, **50**, 1470–1477.
557 53 S. Stølen and T. Grande, *Chemical Thermodynamics of Materials*, Wiley, 2003.
558 54 G. Das, S. Hlushak, M. C. dos Ramos and C. McCabe, Predicting the thermodynamic properties and
559   dielectric behavior of electrolyte solutions using the SAFT-VR+DE equation of state, *AIChE J.*, 2015,
560   **61**, 3053–3072.
561 55 J. Park, W. Lee, J. Kwon Choe and Y. Choi, Non-evaporative solid phase ammonium sulfate separation
562   from ammonia-stripped sulfuric acid solution by solvent-driven fractional crystallization, *Sep. Purif.*
563   *Technol.*, 2023, 123869.
564 56 United States, US20140158616A1, 2014.
565 57 Y. Ma, M. Svärd, X. Xiao, J. M. Gardner, R. T. Olsson and K. Forsberg, Precipitation and Crystallization
566   Used in the Production of Metal Salts for Li-Ion Battery Materials: A Review, *Metals*, 2020, **10**, 1609.
567 58 Y. Wada, M. Matsumoto and K. Onoe, Antisolvent crystallization of NaCl using the minute-bubble
568   technique – Effects of different antisolvent types, *J. Cryst. Growth*, 2016, **448**, 76–81.
569 59 K. L. Pinder, Activity of Water in Solution with Tetrahydrofuran, *J. Chem. Eng. Data*, 1973, **18**, 275–
570   277.
571 60 A. S. Brunjes and M. J. P. Bogart, Vapor-Liquid Equilibria for Commercially Important Systems of
572   Organic Solvents: The Binary Systems Ethanol-n-Butanol, Acetone-Water and Isopropanol-Water, *Ind.*
573   *Eng. Chem.*, 2002, **35**, 255–260.
574 61 L. S. Smith, E. E. Tucker and S. D. Christian, Vapor-density and liquid-vapor equilibrium data for binary
575   mixtures of 2,2,2-trifluoroethanol with water, methanol, ethanol, and 2-butanol, *J. Phys. Chem.*,
576   1981, **85**, 1120–1126.
577 62 R. Macchieraldo, S. Gehrke, N. K. Batchu, B. Kirchner and K. Binnemans, Tuning Solvent Miscibility: A
578   Fundamental Assessment on the Example of Induced Methanol/ n-Dodecane Phase Separation, *J.*
579   *Phys. Chem. B*, 2019, **123**, 4400–4407.
580 63 S. Koley and S. Ghosh, A deeper insight into an intriguing acetonitrile–water binary mixture:
581   synergistic effect, dynamic Stokes shift, fluorescence correlation spectroscopy, and NMR studies,
582   *Phys. Chem. Chem. Phys.*, 2016, **18**, 32308–32318.
583 64 J. J. Shephard, S. K. Callear, S. Imberti, J. S. O. Evans and C. G. Salzmann, Microstructures of negative
584   and positive azeotropes, *Phys. Chem. Chem. Phys.*, 2016, **18**, 19227–19235.
585 65 Y. Marcus, The structure of and interactions in binary acetonitrile + water mixtures, *J. Phys. Org.*
586   *Chem.*, 2012, **25**, 1072–1085.
587 66 R. Sander, Compilation of Henry's law constants (version 4.0) for water as solvent, *Atmospheric*
588   *Chem. Phys.*, 2015, **15**, 4399–4981.
589 67 M. Nagasaka, H. Yuzawa and N. Kosugi, Microheterogeneity in Aqueous Acetonitrile Solution Probed
590   by Soft X-ray Absorption Spectroscopy, *J. Phys. Chem. B*, 2020, **124**, 1259–1265.
591 68 H. T. French, Vapour pressures and activity coefficients of (acetonitrile + water) at 308.15 K, *J. Chem.*
592   *Thermodyn.*, 1987, **19**, 1155–1161.
593 69 T. Takamuku, A. Yamaguchi, D. Matsuo, M. Tabata, M. Kumamoto, J. Nishimoto, K. Yoshida, T.
594   Yamaguchi, M. Nagao, T. Otomo and T. Adachi, Large-Angle X-ray Scattering and Small-Angle Neutron
595   Scattering Study on Phase Separation of Acetonitrile–Water Mixtures by Addition of NaCl, *J. Phys.*
596   *Chem. B*, 2001, **105**, 6236–6245.

597   70 M. Hichri, R. Besbes, Z. Trabelsi, N. Ouerfelli and I. Khattech, Isobaric vapour–liquid phase diagram
598   and excess properties for the binary system 1,4-dioxane + water at 298.15 K, 318.15 K and 338.15 K,
599   *Phys. Chem. Liq.*, 2014, **52**, 373–387.
600   71 E. R. Smith and M. Wojceichowski, Boiling-point-composition digram of the system dioxane-water, ,
601   DOI:10.6028/JRES.018.023.
602   72 A. S. Brunjes and M. J. P. Bogart, Vapor-Liquid Equilibria for Commercially Important Systems of
603   Organic Solvents: The Binary Systems Ethanol-n-Butanol, Acetone-Water and Isopropanol-Water, *Ind.*
604   *Eng. Chem.*, 1943, **35**, 255–260.
605   73 K. L. Pinder, Activity of water in solution with tetrahydrofuran, *J. Chem. Eng. Data*, 1973, **18**, 275–277.
606   74 L. S. Smith, E. E. Tucker and S. D. Christian, Vapor-density and liquid-vapor equilibrium data for binary
607   mixtures of 2,2,2-trifluoroethanol with water, methanol, ethanol, and 2-butanol, *J. Phys. Chem.*,
608   1981, **85**, 1120–1126.
609   75 A. Oleinikova, I. Brovchenko, A. Geiger and B. Guillot, Percolation of water in aqueous solution and
610   liquid–liquid immiscibility, *J. Chem. Phys.*, 2002, **117**, 3296.
611   76 L. B. Pártay, P. Jedlovszky, I. Brovchenko and A. Oleinikova, Formation of mesoscopic water networks
612   in aqueous systems, *Phys. Chem. Chem. Phys.*, 2007, **9**, 1341–1346.
613   77 M. J. Servis, D. T. Wu, J. C. Shafer and A. E. Clark, Reimagining Third Phase Formation as the Miscibility
614   Gap of a Molecular Solution, *ChemRxiv*, , DOI:10.26434/CHEMRXIV.10060253.V1.
615   78 J. Mu, R. Motokawa, K. Akutsu, S. Nishitsuji and A. J. Masters, A Novel Microemulsion Phase
616   Transition: Toward the Elucidation of Third-Phase Formation in Spent Nuclear Fuel Reprocessing, *J.*
617   *Phys. Chem. B*, 2018, **122**, 1439–1452.
618